Large ensemble simulation for investigating predictability of precursor vortices of Typhoon Faxai in 2019 with a 14-km mesh global nonhydrostatic atmospheric model

Yohei Yamada[1], Tomoki Miyakawa[2], Masuo Nakano[1], Chihiro Kodama[1], Akiyoshi Wada[3], Tomoe Nasuno[1], Ying-Wen Chen[2], Akira Yamazaki[1], Hisashi Yashiro[4], and Masaki Satoh[2]

[1]Japan Agency for Marine-Earth Science Technology
[2]Atmosphere and Ocean Research Institute, the University of Tokyo
[3]Meteorological Research Institutes
[4]National Institute for Environmental Studies

November 25, 2022

Abstract

Typhoon Faxai hit Japan in 2019 and severely damaged the Tokyo metropolitan area. To mitigate such damages, a good track forecast is necessary even before the typhoon formation. To investigate the predictability of the genesis and movement of a precursor vortex and its relationship with the synoptic-scale flow, 1600-member ensemble simulations of Typhoon Faxai were performed using a 14-km mesh global nonhydrostatic atmospheric model, which started from 16 different initial days (i.e., 1600 members in total). The results show that the model could predict an enhanced risk of a Faxai-like vortex heading toward Japan two weeks before landfall, which was up to 70%. The reason for the enhancement was a rapid increase in the members reproducing a precursor vortex from 15 to 12 days before landfall in Japan. In addition, the upper-tropospheric trough played an essential role in the track simulation of Faxai.

Large ensemble simulation for investigating predictability of precursor vortices of Typhoon Faxai in 2019 with a 14-km mesh global nonhydrostatic atmospheric model

Y. Yamada[1], T. Miyakawa[2], M. Nakano[1], C. Kodama[1], A. Wada[3], T. Nasuno[1], Y. Chen[2], A. Yamazaki[1], H. Yashiro[4], M. Satoh[2]

[1]Japan Agency for Marine-Earth Science and Technology.

[2]Atmosphere and Ocean Research Institute, the University of Tokyo.

[3]Meteorological Research Institutes, Japan Meteorological Agency.

[4]National Institute for Environmental Studies.

Corresponding author: Yohei Yamada (yoheiy@jamstec.go.jp)

Key Points:

- A 1600-member ensemble simulation for Typhoon Faxai (2019) was performed using a 14-km mesh nonhydrostatic atmospheric model.
- The model successfully predicts the risk of Faxai's landfall in Japan two weeks in advance.
- Reproducibilities of the precursor vortex and upper-tropospheric trough yield good prediction of the formation and track of Faxai.

Abstract

Typhoon Faxai hit Japan in 2019 and severely damaged the Tokyo metropolitan area. To mitigate such damages, a good track forecast is necessary even before the typhoon formation. To investigate the predictability of the genesis and movement of a precursor vortex and its relationship with the synoptic-scale flow, 1600-member ensemble simulations of Typhoon Faxai were performed using a 14-km mesh global nonhydrostatic atmospheric model, which started from 16 different initial days (i.e., 1600 members in total).

The results show that the model could predict an enhanced risk of a Faxai-like vortex heading toward Japan two weeks before landfall, which was up to 70%. The reason for the enhancement was a rapid increase in the members reproducing a precursor vortex from 15 to 12 days before landfall in Japan. In addition, the upper-tropospheric trough played an essential role in the track simulation of Faxai.

Plain Language Summary

Tropical cyclones severely damage coastal regions yearly. Typhoon Faxai hit Japan in 2019 and severely damaged buildings, power grids, and cell phone networks in the Tokyo metropolitan area. To mitigate such damages, better track forecast is necessary even from the timing before typhoon formation. A large ensemble member (1600-member) and high-resolution (14-km) simulation was performed to investigate the genesis and movement of the precursor vortex of Faxai in 2019 and its relationship with the synoptic-scale environmental flow using a global nonhydrostatic atmospheric model on the Supercomputer Fugaku.

The results show the model could predict an enhanced risk of a Faxai-like vortex heading toward Japan two weeks before landfall. A reason for the enhancement was a rapid increase in the members reproducing a precursor vortex from 15 to 12 days before landfall in Japan. In addition, the upper-tropospheric trough played an essential role in the movement of the Faxai-like vortex.

1 Introduction

A tropical depression developed into a tropical cyclone (TC) named Faxai at 18 UTC on September 4, 2019, at 18.6°N, 156.7°E, according to the Regional Specialized Meteorological Center-Tokyo best track (RSMCBT). Faxai moved northwestward and reached a central pressure of 955 hPa at 18 UTC on September 7. Faxai made landfall in the Tokyo metropolitan area of Japan at 17 UTC on September 8. The relatively small TC caused very strong winds, particularly in the metropolitan area, tremendously damaging buildings, power grids, and cell phone networks (Japan Meteorological Agency, 2020; Miyamoto et al., 2022; Fudeyasu et al., 2022). A remarkable feature of Faxai was that there were only approximately four days from the genesis to the landfall (Fudeyasu et al., 2022).

To mitigate disasters associated with TCs, predicting a long lead time (LT) is necessary, which requires good forecasts for TC formation and track, as well as precursor vortices. Nakano et al. (2015) demonstrated that TC formation can be predicted two weeks in advance. However, the track forecast after TC formation has not been investigated. In addition, although operational numerical weather forecast models improve TC track forecasts, challenges such as enhanced use of ensemble remain (Yamaguchi et al., 2017).

A TC track is largely controlled by a synoptic-scale flow (Chan, 2017; Ito et al., 2020). Regarding the influence of synoptic-scale flow, Fudeyasu et al. (2022) mentioned that the upper-tropospheric cold low (UTCL) approached a precursor vortex of Faxai. Wei et al. (2016) showed that UTCLs can affect a TC track, depending on their relative distance and orientation. TCs in a UTCL's southern half are more likely to intensify, whereas those in the northern half are more likely to weaken; also, TCs in a UTCL's northeastern quadrant tend to weaken more slowly than those in the western North Pacific climatology (Wei et al., 2016; Wada et al., 2022). By performing ensemble simulations from different initial times, Wada et al. (2022) noted that variations in atmospheric initial conditions yield variations in the effect of cut-off lows on TC track simulations.

Previous studies have suggested that ensemble simulations improve TC track forecasts (Nakano et al., 2017; Magnusson et al., 2019). In addition, the use of high-resolution global models in which convective storms are explicitly resolved further improves TC track forecasts (Nakano et al., 2017; Yamada et al., 2016). To the best of our knowledge, large-number ensemble experiments (e.g., ensemble size >100 from each initial time) using such high-resolution models have not been performed, except by Nakano et al. (2022).

The Fugaku, a recently developed pre-exascale supercomputer in Japan, opens the door to examine the predictability of TC tracks, even before its formation. In this study, we demonstrate the effectiveness of large-member ensemble experiments with horizontal high-resolution in predicting the occurrence of disasters due to the landfall of Faxai in Japan and then clarify the predictability of the genesis and movement of the precursor vortices of Faxai and their relationships with synoptic-scale flows.

2 Experiments and data

2.1 1600-member ensemble simulation for Faxai

2.1.1 Experimental setting

We performed high-resolution large ensemble simulations for Faxai with 1600 ensemble members. The Nonhydrostatic ICosahedral Atmospheric Model (NICAM) (Tomita & Satoh, 2004; Satoh et al., 2008, 2014) was used for the simulations with a 14-km horizontal mesh. The configuration of the model was almost the same as that of Kodama et al. (2021). The aerosol effect was not considered; using a slab ocean model with a 15-m depth, sea surface temperature (SST) was calculated and nudged toward National Oceanic and Atmospheric Administration daily optimum interpolation SST Version 2.1 (Huang et al., 2020) with a relaxation time of one week. The atmospheric initial conditions were developed from NICAM-Local Ensemble Transform Kalman Filter (LETKF) Japan Aerospace Exploration Agency (JAXA) Research Analysis (NEXRA) (Kotsuki et al., 2019) dataset. The number of ensemble members in NEXRA was 100 every 6 h with a 1.25° horizontal resolution. We used all the 100 members of NEXRA at 18 UTC each day from August 20 to September 4, 2019 (16 days). Thus, a 1600-member ensemble simulation was performed to investigate the predictability of Faxai.

Faxai traversed Tokyo Bay at 18 UTC on September 8, 2019, referred to as the approaching time in this study. An LT was defined with reference to the approaching time, and the 1600-member ensemble simulation covered LTs from “LT04” (starting from September 4) to “LT19” (starting from August 20), with 100-member runs for each LT.

2.1.2 Extracting Faxai-like vortex

To detect vortices like Faxai in our ensemble simulation, we employed a TC tracking method modified from Nakano et al. (2015), which is described in Supporting Information Text S1. In this study, we analyzed not only TC but also tropical depressions. Next, we selected Faxai-like vortices from extracted tracks. We regard a vortex traversing within a 1000-km radius from the genesis location of the real Faxai within 5 days before and after its genesis time (criterion B) as a Faxai-like vortex. In addition, we extracted vortices approaching Japan from Faxai-like vortices, which traversed within a 1000-km radius from Tokyo Bay within 5 days before and after the time when the real Faxai existed over Tokyo Bay (criterion A). We classified Faxai-like vortices into two types of vortices: type-AB vortex (satisfying both criteria A and B) and type-B vortex (satisfying only criteria B). Supporting Information Text S2 provides more details, and Supporting Information Fig. S1 shows the samples of tracks for type-AB and type-B vortices. In this study, vortices were classified and named based on some condition. The names of the classified vortices are listed in Supporting Information Table S1.

2.2 NICAM climatology ensemble simulation

A global atmospheric model predicts a different mean state from the analysis, as the forecast time becomes longer (Vitart, 2014). For instance, Roberts et al. (2020) showed that NICAM overestimated TC using a diagram. To clarify that our Faxai ensemble simulation results are not given by such overestimation in NICAM, the results need to be compared with NICAM's model climatology.

2.2.1 Experimental setting

To derive NICAM's model climatology, 64-member ensemble simulations were performed from 2009 to 2019 with a time-slice framework (Kinter et al., 2013). These simulations started from August 20, except for 2015. In 2015, the initial time was used as August 19 because of numerical instability. The simulations were performed until September 30 (approximately 40 days). The atmospheric initial conditions were created from the Atmospheric General Circulation Model for the Earth Simulator–LETKF experimental ensemble reanalysis 2 (ALERA2; Enomoto et al., 2013). The experimental setting was the same as that in the 1600-member ensemble simulation for Faxai.

2.2.2 Extracting Faxai-like vortices

Vortex tracks were detected in the NICAM climatology ensemble simulation using the almost same method as in the 1600-member ensemble simulation for Faxai (Supporting Information Text S1). Because Faxai 2019 was generated in early September 2019, we assumed vortices generated in early September 2019 in the climatology ensemble simulations as Faxai-like vortices. The NICAM climatology ensemble simulations were run for a specific initial date each year, unlike the 1600-member ensemble simulation for Faxai. Although Faxai-like vortices were selected from the track data using the same method as in the 1600-member ensemble simulation for Faxai (Supporting Information Text S2), the genesis time was shifted from September 1 to 20 for each ensemble member. To distinguish type-AB vortex from type-B vortex, criterion A was applied to the Faxai-like vortices with the time lag between the genesis and approaching times fixed to 4 days. The averages of the numbers were used as the climatology of the genesis probability of type-AB and type-B vortices in early September.

2.3 Data

The RSMCBT and early-stage Dvorak analysis data (EDA) provided by the Japan Meteorological Agency (JMA; Kishimoto, 2008) were used as the reference locations of Faxai. Because, In the RSMCBT, the real Faxai was generated at 18 UTC on September 4, 2019, we called the real precursor vortex of Faxai Pre-Faxai. The location of Pre-Faxai before the EDA was extracted from a reanalysis. The fifth-generation European Centre for Medium-Range Weather Forecasts (ECMWF) atmospheric reanalysis (ERA5; Hersbach, 2020) was employed in this study.

The same method as in the ensemble experiment was used for extracting Faxai's vortices from ERA5. Pre-Faxai in ERA5 could be detected as far back as 06 UTC on August 24, 2019 (Fig. 1a)

The results of the ensemble simulations with the 1.25° horizontal resolution regridded from the original resolution were used to analyze the atmospheric environments of TCs.

3 Results

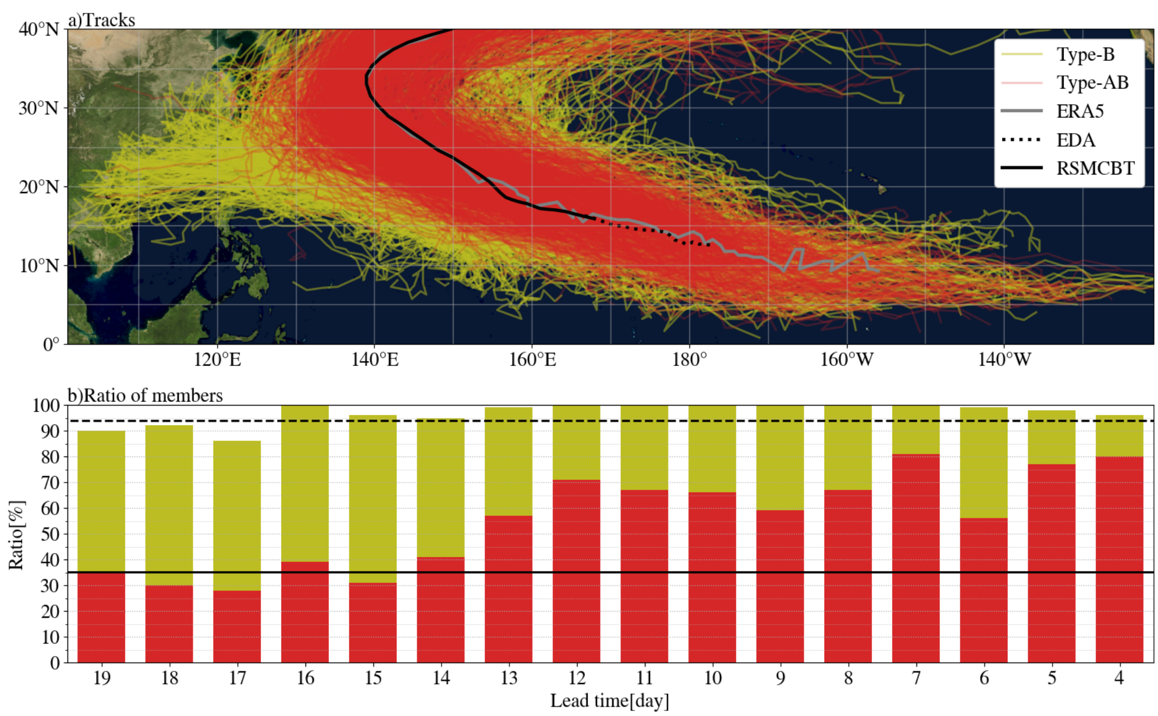

Figure 1. (a) Plan view of simulated tracks of Faxai-like vortices in a 1600-member Faxai ensemble simulation. The red and yellow lines denote the tracks of type-AB and type-B vortices, respectively. The black solid, black dashed, and solid gray lines denote the RSMCBT, EDA, and ERA5, respectively. Topography and bathymetry are Blue Marble: Next generation (September) which was produced by Reto Stöckli, NASA Earth Observatory. (b) Ratio of ensemble members reproducing Faxai-like vortices to respective 100 members for each LT. The red and yellow bars indicate the rates of those reproducing type-AB and type-B vortices, respectively, for each LT. The solid and dashed lines denote the mean rate of the ensemble members reproducing type-AB and type-B vortices, respectively, in NICAM climatology ensemble simulation.

First, we show tracks of Faxai-like vortices extracted from the 1600 Faxai's ensemble simulation (Fig. 1a). As expected, type-AB vortex tended to approach Japan, whereas type-B vortex seemed to travel westward, eastward, or took a larger detour before moving northward and then traveled toward Japan. Figure 1b shows the percentages of members with Faxai-like vortices exceeding 85% for all LT and the number of members with type-AB vortex increasing conspicuously from LT15 to LT12, instead of a decrease in members with type-AB vortex for LT06.

Next, we compared the Faxai's ensemble simulation results with those of the climatology ensemble simulation to determine whether the number of members with Faxai-like vortices changed due to systematic forecast drifts in the model or the influence of the specific environment in 2019. In the climate ensemble simulations, a Faxai-like vortex was generated in approximately 95% of members, and type-AB vortex was formed in 35% of members. In other words, about 37% of Faxai-like vortices moved toward Japan. Overall, the ratio of the number of members with the Faxai-like vortices in the Faxai's ensemble simulations was higher than that in the model climatology after LT16. After LT13, the ratio of the number of members with type-AB vortex was higher than that in the model climatology. From the comparison results, the conspicuous increase in the number of members with type-AB vortex in the Faxai's ensemble simulations was not due to systematic drifts but due to the influence of the specific environment in 2019. In summary, NICAM could predict with high accuracy two weeks before landfall that the vortex was likely to head toward Japan.

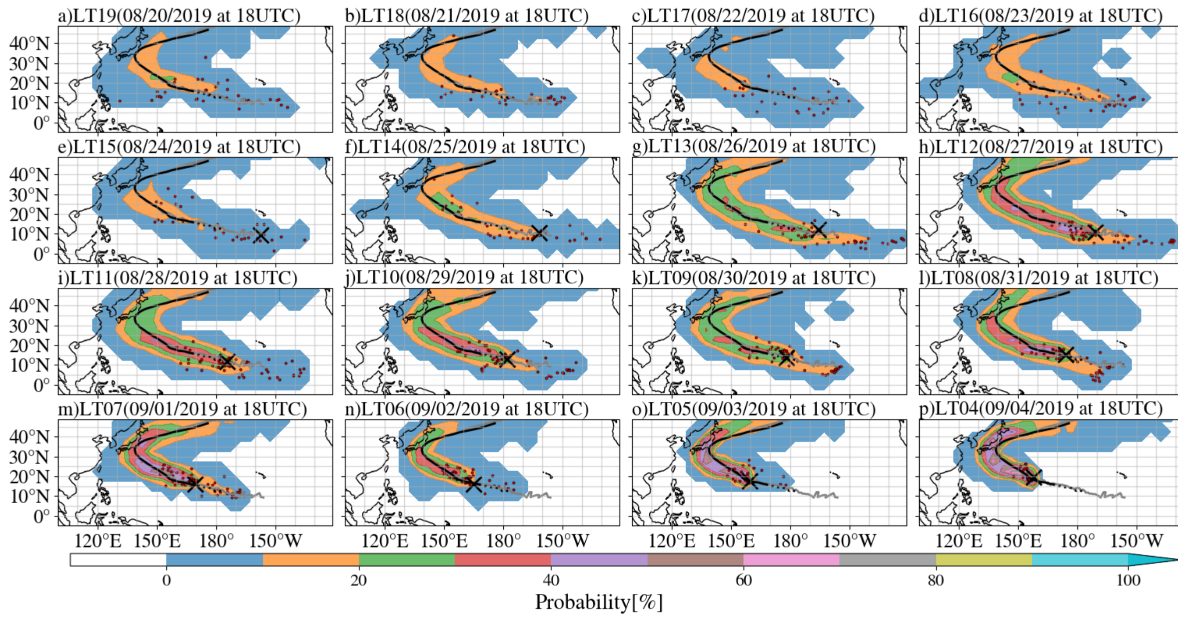

Figure 2. Plan views of strike probability density for type-AB vortex for each 100-member simulation starting from each LT. The density is defined by vortices per 5° cap. The black solid, black dashed, and solid gray lines denote the RSMCBT, EDA, and ERA5, respectively. The figure in parentheses indicates the start time of each 100-member ensemble simulation. The cross symbol indicates the location of Pre-Faxai (e–o) or Faxai (p) at the start time for each LT. These locations were determined from ERA5. The red circles indicate the starting points of tracks of type-AB vortex.

Figure 2 shows the horizontal distribution of strike probability density for type-AB vortex by each LT (LT19–LT04). For every LT, the strike probability exceeded 10% around the RSMCBT. From LT15 to LT12, the strike probabilities increased systematically around the RSMCBT. Although the strike probability in LT11 decreased in the vicinity of east Japan compared with that in LT12, the strike probability became higher in the vicinity of east Japan with a shorter LT, indicating that the track of type-AB vortex in the simulation starting from a short LT became close to the real Faxai track. Figure 2 also shows the starting positions of members with type-AB vortex. Although the starting positions were sparse for LT19–LT16, they appeared to become denser along the real Faxai track as the LT became smaller, suggesting that the representation of vorticity was sensitive to LT, which seemed to contribute to the increase in the number of members with type-AB vortex between LT15 and LT12.

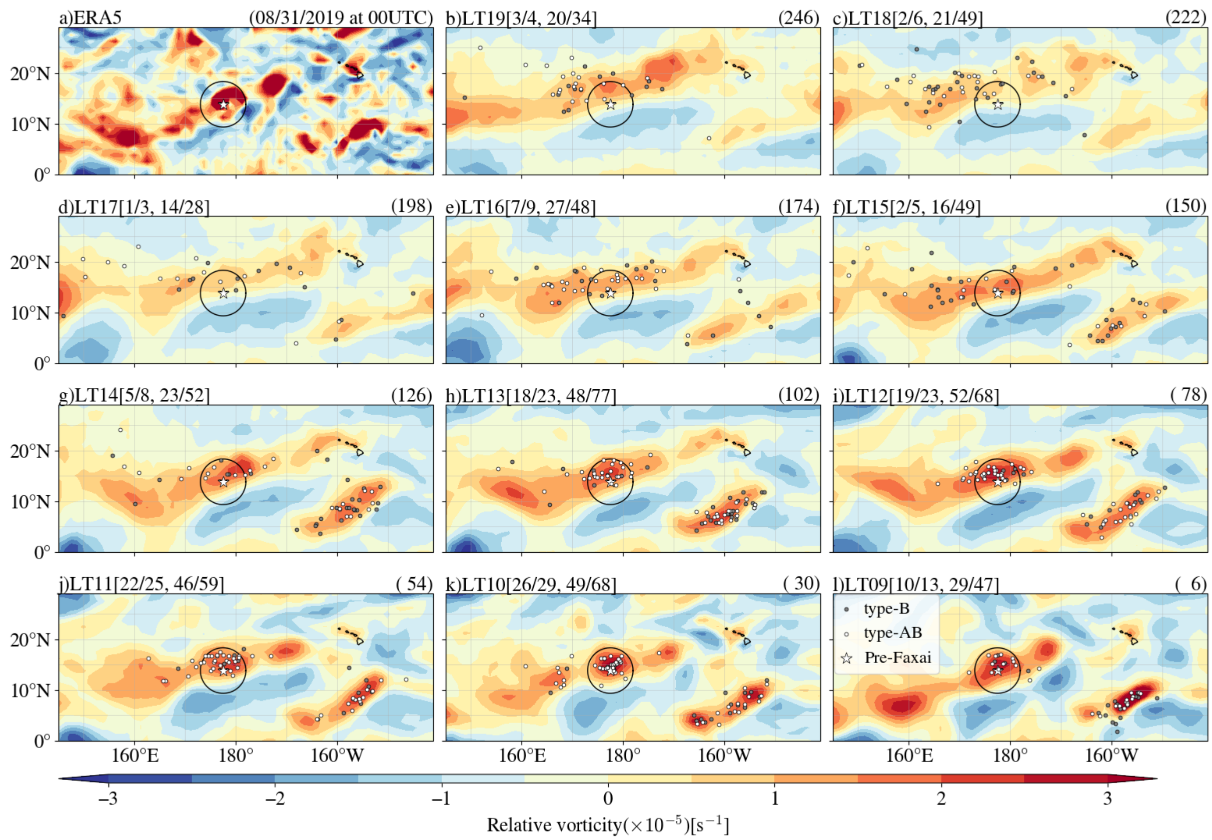

Figure 3. Plan views of the relative vorticity at 850 hPa at 00 UTC on August 31, 2019 for ERA5 (a) and those in the 100-member ensemble mean for LT19 to LT9 (b–l). Numerals in parentheses on the upper-right side of panels (b–l) indicate forecast time [h]. Positions of type-B and type-AB vortices at 00 UTC on August 31, 2019, in each LT are embedded on each panel with black and white circles, respectively. The star-shaped symbol denotes the position of Pre-Faxai analyzed in the EDA at 00 UTC on August 31. The figures in square brackets indicate the numbers of type-AB/Faxai-like vortices within the surrounding circle and those in the domain. The number of Faxai-like vortices is the sum of the numbers of type-B and type-AB vortices.

Figure 3 shows the 100-member ensemble composite of relative vorticity at 850 hPa and positions of Faxai-like vortices at 00 UTC on August 31 for LT19–LT09 to investigate why the number of members with type-AB vortex increased after LT15. The relative vorticity became stronger around Pre-Faxai based on the EDA as the LT became shorter. As for the Faxai-like vortices within a 500-km radius of Pre-Faxai and within the domain, their numbers varied with the LT, which seems to be complicated. The vortices seem to be spontaneously generated in the simulation or included in the initial condition and maintained under favorable environmental conditions. The former may increase over the forecast time, and the latter may increase with the LT becoming shorter. However, the numbers increased rapidly from LT15 to LT12, which were more than four times (from 5 to 23) within a 500-km radius of Pre-Faxai and approximately 1.4 times (from 49 to 68) within the domain. This can contribute to the rapid increase in type-AB vortex from LT15 to LT12. In summary, an accurate forecast of a precursor vortex is a key factor for a good forecast of Faxai.

With respect to the differences in the tracks between type-AB and type-B vortices, members with type-AB vortex traveled northwestward toward Japan (Fig. 2), whereas most members with type-B vortex traveled westward, took a larger detour before moving northward, and then traveled toward Japan (Supporting Information Fig. S2). Next, we address the reason for differences in tracks between type-AB and type-B vortices. Figure 1a shows that the track of a vortex changed from west–northwest to northwest near 160°E. As the members with type-AB vortex increased after LT15, we composite the members with type-AB and type-B vortices from LT15 to LT08 and compare their synoptic environments before those vortices reached 160°E. Figure 3 shows that the locations of the Faxai-like vortices are roughly divided into two regions: around Pre-Faxai (near 15°N, 178°E) and its southeast side (near 10°N, 155°W). Each vortex seems to be affected by differences in synoptic-scale flow. For ease in comparison between type-AB and type-B vortices, we ignored ensemble members with Faxai-like vortices being the southeast side of Pre-Faxai. We excluded the members whose starting location of the track was 5° east far from the location detected in ERA5 at the same time.

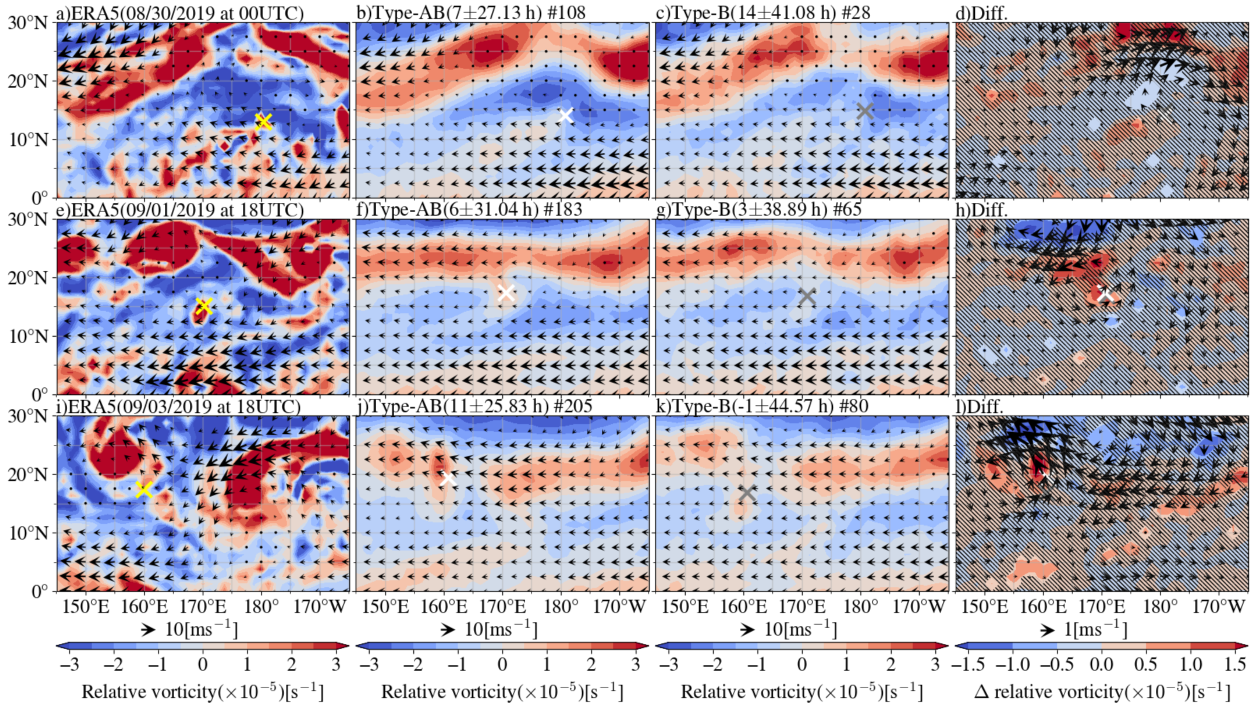

Figure 4. Plan views of relative vorticity at a 300-hPa and steering flow when the vortices existed at 180°: (a) ERA5, (b) type-AB vortex composite, (c) type-B vortex composite, and (d) difference between type-AB and type-B vortices when the mean longitude of vortices was approximately 180°. (e–h) The same as (a–d), respectively, but for 170°E. (i–l) The same as (a–d), respectively, but for 160°E. The yellow cross denotes the positions of Pre-Faxai analyzed in the EDA (a and e) and Faxai analyzed in the RSMCBT (i). The white and gray crosses indicate the ensemble mean positions of type-AB and type-B vortices, respectively. The hatch indicates regions in which differences between type-AB and type-B vortices are statistically not significant at 95% with the Welch t-test. The panels for ERA5 show the date at the top. The panels for type-AB and type-B vortex composites show the mean time difference from the date of ERA5 with the standard deviation at the top. The integers on the right side of the sharp mark indicate the numbers of ensemble members in each composite case.

As Fudeyasu et al. (2022) showed the influence of UTCL on Faxai, we focused on the upper-level vorticity and steering flow. The steering flow was calculated using the formula of Colbert and Soden (2012) after moving averages were evaluated over a rectangular area of 10° × 10°. The upper, middle, and lower panels in Fig. 4 show the horizontal distribution of relative vorticity at the 300-hPa and steering flow when the vortices existed at 180°, 170°E, and 160°E, respectively.

When the vortex is located around 180° (Figs. 4a–4c), a westward steering flow existed at the south of the vortex. Meanwhile, the steering flow was weak in the north of the vortex. The north of 15°N is a region with the positive vorticity zonally extended with meandering. The positive vorticity region corresponds to the tropical upper-tropospheric trough (TUTT). The difference in the upper-level flows between the type-AB and type-B vortex composites is statistically not significant in most areas around the vortices (Fig. 4d).

When the vortex moved further west and reached 170°E (Figs. 4e–4g), the distance from the TUTT to the vortices except for type-B vortex composite reduced. The difference in the relative vorticity between type-AB and type-B vortex composites was significant (Fig. 4h). The difference in the steering flow deflected northeastward, indicating that type-AB vortex tended to travel northward compared with type-B vortex.

At the arrival time of the vortex around 160°E, it was confirmed that type-AB vortex had been coupled with the upper-tropospheric vortex (Fig. 4j), the same as in the ERA5 field (Fig. 4i). In addition, a positive vorticity maximum is located just over the west of type-AB vortex; therefore, type-AB vortex can be steered toward northwestward. However, this feature cannot be confirmed for the type-B vortex composite (Fig. 4k); thus, the vortex traveled westward without heading northward. The location of TUTT could have separated the tracks between type-AB and type-B vortices, whether the vortex headed toward Japan (type-AB vortex) or not (type-B vortex).

4 Discussions

For precursor vortices that approached Japan (type-AB), their movement tended to be forced by southerly steering flow when they existed from 180° to 160°E (Fig. 4). This southerly steering flow may be induced by a TUTT or cut-off low (Wei et al., 2016). When a TUTT or cut-off low exists on the northwest side of a TC, the vertical wind shear becomes weakened around the TC (Wei et al., 2016). The relatively small vertical wind shear is a favorable environment for TC formation, which agrees with our result that a precursor vortex was more intensified in type-AB (24.4 ± 10.5 ms^{-1}) than in type-B (17.0 ± 7.0 ms^{-1}) when the vortices arrived at 160°E. However, Fudeyasu et al. (2022) reported that the intensification of Faxai was suppressed by a cut-off low due to an increase in vertical wind shear near the cut-off low. The reason for this inconsistency with our results is unclear. Wei et al. (2016) noted that TC intensification near a cut-off low depends on the relative location and distance because of the interaction between a TC and cut-off low. This is a topic for future work, and it would be possible to quantify the interaction because the high-resolution large ensemble experimental results can be obtained based on our technique.

Another discussion is on the origin of type-AB vortex. Figures 3f–l show two clusters of Faxai-like vortices. The first cluster was located around Pre-Faxai, which could be regarded as the correct vortex. The second vortex cluster was located on the southeast side of Pre-Faxai, which could be regarded as another vortex (possible vortex). The possible vortex increased from LT15 and decreased from LT08, whereas the correct vortex increased as the LT became shorter (Supporting Information Fig. S3). The compensation between possible and correct vortices can contribute to the decrease in the number of ensemble members with type-AB vortex at LT06 shown in Fig. 1b. Moreover, this result suggests that two kinds of the precursor vortices developed into a typhoon and approached Japan. In Fig. 3, because ERA5 also shows a relatively strong vortex on the southeast side of Pre-Faxai, the possible vortex seems to be not fully unreasonable. TCs that originated from the possible vortex and approached Japan tended to arrive near Japan later and became stronger than those that originated from correct vortices (Supporting Information Figs. S4 and S5). The delayed arrival was because the possible vortex tended to travel from farther south−eastward (Fig. 2 and Supporting Information Fig. S2), whereas the long duration over warm water yielded intense TCs, as documented by Camargo and Sobel (2006).

5 Summary and Concluding remarks

A high-resolution large-member ensemble simulation was performed for Typhoon Faxai 2019, which caused a severe disaster, particularly in the Tokyo metropolitan area. We found that the risk of Faxai approaching Japan was enhanced two weeks before the landfall in Japan. Detailed data analysis showed that the ensemble simulation covers not only the scenario that Faxai developed from a precursor vortex in the western positively vortical area (near 180° in Fig. 3) as in reality but also a potential scenario in which a similar but a later and stronger TC approaches Japan, formed at a different area far southeast of the real vortex.

A reason for the increase in the number of ensemble members with type-AB vortex from two weeks in advance was a rapid increase in the number of members with the precursor vortex from LT15 to LT12. In addition, the TUTT played an essential role in the track simulation of Faxai. The result suggests the accurate simulation of the TUTT and associated cut-off low is crucial for simulating an accurate track of Faxai by improving steering flow.

Acknowledgments

This research used computational resources of the supercomputer Fugaku by the RIKEN (ID: hp200128, hp210166, hp220167) supported by Ministry of Education, Culture, Sports, Science and Technology (JPMXP1020351142) as “Program for Promoting Researches on the Supercomputer Fugaku” (Large Ensemble Atmospheric and Environmental Prediction for Disaster

Prediction and Mitigation). NEXRA used for the initial conditions for 1600-member ensemble simulation is provided by JAXA. The RSMCBT and EDA data are provided by JMA. ERA5 is provided by ECMWF via the Copernicus Climate Change Service Climate Data Store. The authors would like to thank Enago (www.enago.jp) for English language review.

Open Research

RSMCBT is available at (https://www.jma.go.jp/jma/jma-eng/jma-center/rsmc-hp-pub-eg/besttrack.html); The EDA used in this study is available at Supporting Information Table S1; ERA5 is available at (https://www.ecmwf.int/en/forecasts/datasets/reanalysis-datasets/era5); NEXRA is available at (https://www.eorc.jaxa.jp/theme/NEXRA/guide.htm); ALERA2 is available at (https://www.jamstec.go.jp/alera/alera2.html). NICAM simulation data and vortex tracking code used in this study are available at (Yamada, 2022, https://zenodo.org/record/6889432). The model source code is shared with the NICAM community and available at (Kodama et al., 2020, https://zenodo.org/record/3727329) as long as the user follows the terms and condition on (http://nicam.jp/hiki/?Research+Collaborations). Figures were plotted by using Matplotlib (https://matplotlib.org/stable/index.html), Cartopy (Met Office, 2022, https://zenodo.org/record/6775197), MetPy (May et al., 2022, https://www.unidata.ucar.edu/software/metpy/), and SciPy (Virtanen et al., 2020, https://scipy.org/).

References

Camargo, S. J., & Sobel, A. H. (2005), Western North Pacific tropical cyclone intensity and ENSO. *Journal of Climate*, *18*(15), 2996–3006. doi:10.1175/JCLI3457.1

Chan, J. C. L. (2017). Physical mechanisms responsible for track changes and rainfall distributions associated with tropical cyclone landfall. Oxford Handbooks Online, doi:10.1093/oxfordhb/9780190699420.013.16

Colbert, A. J., & Soden, B. J. (2012), Climatological variation in North Atlantic tropical cyclone tracks, *Journal of Climate*, *25*(2), 657–673. doi:10.1175/JCLI-D-11-00034.1

Enomoto, T., Miyoshi, T., Moteki, Q., Inoue, J., Hattori, M., Kuwano–Yoshida, A., Komori, N., & Yamane, S. (2013). Observing-system research and ensemble data assimilation at JAMSTEC. In: Park, S., Xu, L. (Eds.), *Data Assimilation for Atmospheric, Oceanic and Hydrologic Applications* (Vol. 2, pp. 509–526). Berlin, Heidelberg: Springer. doi:10.1007/978-3-642-35088-7_21

Fudeyasu, H., Shimada, U., Oikawa, Y., Eito, H., Wada, A., Yoshida, R., & Horinouchi, T. (2022). Contributions of the large-scale environment to the typhoon genesis of Faxai (2019). *Journal of the Meteorological Society of Japan*, *100*(4). doi:10.2151/jmsj.2022-031

Hersbach, H., Bell, B., Berrisford, P., Hirahara, S., et al. (2020). The ERA5 global reanalysis. *Quarterly Journal of the Royal Meteorological Society, 146*(730), 1999–2049. doi:10.1002/qj.3803

Huang, B., Liu, C., Banzon, V., Freeman, E., Graham, G., Hankins, B., Smith, T., & Zhang, H.-M. (2021). Improvements of the Daily Optimum Interpolation Sea Surface Temperature (DOISST) Version 2.1. *Journal of Climate*, *34*(8), 2923–2939. doi:10.1175/JCLI-D-20-0166.1

Ito, K., Wu, C.-C., Chan, K. T. F., Toumi, R., & Davis, C. (2020). Recent progress in the fundamental understanding of tropical cyclone motion. *Journal of the Meteorological Society of Japan. Ser. II,*, *98*(1), 5–17. doi:10.2151/jmsj.2020-001

Japan Meteorological Agency (JMA). (2020). Annual Report on the Activities of the RSMC Tokyo–Typhoon Center 2019. Retrieved from https://www.jma.go.jp/jma/jma-eng/jma-center/rsmc-hp-pub-eg/AnnualReport/2019/Text/Text2019.pdf

Kinter, J. L., III, Cash, B., Achuthavarier, D., Adams, J., Altshuler, E., Dirmeyer, P., et al. (2013). Revolutionizing climate modeling with Project Athena: A multi-institutional, international collaboration. *Bulletin of American Meteorological Society*, 94(2), 231–245. doi:10.1175/BAMS-D-11-00043.1

Kishimoto, K. (2009). Revision of JMA's early stage Dvorak analysis and its use to analyze tropical cyclones in the early developing stage (Technical Review, No. 10). Tokyo, Japan: RSMC Tokyo–Typhoon Center. Retrieved from https://www.jma.go.jp/jma/jma-eng/jma-center/rsmc-hp-pub-eg/techrev/text10-1.pdf

Kodama, C., Ohno, T., Seiki, T., Yashiro, H., Noda, A. T., Nakano, M., et al. (2021). The Nonhydrostatic ICosahedral Atmospheric Model for CMIP6 HighResMIP simulations (NICAM16-S): experimental design, model description, and impacts of model updates, *Geoscientific Model Development*, *14*(2), 795–820. doi:10.5194/gmd-14-795-2021

Kodama, C., Ohno, T., Seiki, T., Yashiro, H., Noda, A. T., Nakano, M., et al. (2020). The Nonhydrostatic ICosahedral Atmospheric Model for CMIP6 HighResMIP simulations (NICAM16-S) [Software]. Zenodo. https://zenodo.org/record/3727329

Kotsuki, S., Terasaki, K., Kanemaru, K., Satoh, M., Kubota, T., & Miyoshi, T., (2019). Predictability of record-breaking rainfall in Japan in july 2018: Ensemble forecast experiments with the near-real-time global atmospheric data assimilation system NEXRA. *Scientific Online Letters on the Atmosphere*, *15*, 1–7. doi:10.2151/sola.15A-001

Magnusson, L., Doyle, J. D., Komaromi, W. A., Torn, R. D., Tang, C. K., Chan, J. C. L., Yamaguchi, M., & Zhang, F. (2019). Advances in understanding difficult cases of tropical cyclone track forecasts. *Tropical Cyclone Research and Review, 8*(2), 109–122. doi:10.1016/j.tcrr.2019.10.001

May, R. Arms, M., Marsh, S. C., Bruning, P., Leeman, E., Goebbert, J. R., et al. (2022). MetPy: A Python Package for Meteorological Data version 1.3.0 [Software]. Unidata, https://doi.org/10.5065/D6WW7G29

Met Office. (2022). SciTools/cartopy: v0.20.3 [Software]. Zenodo. https://doi.org/10.5281/zenodo.1182735

Miyamoto, Y., Fudeyasu, H., & Wada, A. (2022). Intensity and structural change of numerically simulated Typhoon Faxai (1915) before landfall. *Journal of the Meteorological Society of Japan, Ser. II, 100*(1), 181–196. doi:10.2151/jmsj.2022-009

Nakano, M., Sawada, M., Nasuno, T., & Satoh, M. (2015), Intraseasonal variability and tropical cyclogenesis in the western North Pacific simulated by a global nonhydrostatic atmospheric model. *Geophysical Research Letters, 42*(2), 565–571. doi:10.1002/2014GL062479

Nakano, M., Wada, A., Sawada, M., et al. (2017). Global 7-km mesh nonhydrostatic model intercomparison project for improving typhoon forecast (TYMIP-G7): Experimental design and preliminary results. *Geoscientific Model Development*, *10*(3), 1363–1381. doi:10.5194/gmd-10-1363-2017

Nakano, M., Chen, Y.-W., & Satoh, M. (2022). Analysis of the factors that led to an uncertainty of track forecast of Typhoon Krosa (2019) by 101-member ensemble forecast experiments using NICAM. Jxiv. doi:10.51094/jxiv.46

Roberts, M. J., Camp, J., Seddon, J., Vidale, P. L., Hodges, K., Vannière, B., et al. (2020). Projected future changes in tropical cyclones using the CMIP6 HighResMIP multimodel ensemble. *Geophysical Research Letters*, *47*(14), e2020GL088662. doi:10.1029/2020GL088662

Satoh, M., Matsuno, T., Tomita, H., Miura, H., Nasuno, T., & Iga, S. (2008) Nonhydrostatic icosahedral atmospheric model (NICAM) for global cloud resolving simulations. *Journal of the Computational Physics*, *227*(7), 3486–3514. doi:10.1016/j.jcp.2007.02.006

Satoh, M., Tomita, H., Yashiro, H., Miura, H., Kodama, C., Seiki, T., et al. (2014). The non-hydrostatic icosahedral atmospheric model: Description and development. *Progress in Earth and Planetary Science, 1*(1)*,* 18. doi:10.1186/s40645-014-0018-1

Tomita, H., & Satoh, M. (2004). A new dynamical framework of nonhydrostatic global model using the icosahedral grid. *Fluid Dynamics Research*, *34*(6), 357–400. doi:10.1016/j.fluiddyn.2004.03.003

Virtanen, P., Gommers, R., Oliphant, T. E., Haberland, M., Reddy, T., Cournapeau, D., et al., (2020) SciPy 1.0: Fundamental Algorithms for Scientific Computing in Python. *Nature Methods*, 17(3), 261–272. Doi:10.1038/s41592-019-0686-2

Vitrat, F. (2014). Evolution of ECMWF sub-seasonal forecast skill scores. *Quarterly Journal of the Royal Meteorological Society*, *140*(683), 1889–1899. doi:10.1002/qj.2256

Wada, A., Yanase, W., & Okamoto, K. (2022). Interactions between a tropical cyclone and upper-tropospheric cold-core lows simulated by an atmosphere-wave-ocean coupled model: A case study of Typhoon Jongdari (2018). *Journal of the Meteorological Society of Japan. Ser. II,*, *100*(2), 387–414. doi:10.2151/jmsj.2022-019

Wei, N., Li, Y., Zhang, D., Mai, Z., & Yang, S. (2016). A statistical analysis of the relationship between upper-tropospheric cold low and tropical cyclone track and intensity change over the western North Pacific. *Monthly Weather Review*, *144*(5), 1805–1822, doi:10.1175/MWR-D-15-0370.1

Yamada, H., Nasuno, T., Yanase, W., & Satoh, M. (2016). Role of the vertical structure of a simulated tropical cyclone in its motion: a case study of typhoon Fengshen (2008). *Scientific Online Letters on the Atmosphere*, *12*, 203–208, doi:10.2151/sola.2016-041

Yamada, Y. (2022). Data used in a manuscript entitled "Large ensemble simulation for investigating predictability of precursor vortices of Typhoon Faxai in 2019 with a 14-km mesh global nonhydrostatic atmospheric model" submitted to Geophysical Research Letters [Dataset]. Zenodo. https://doi.org/10.5281/zenodo.6889432

Yamaguchi, M., Ishida, J., Sato, H., & Nakagawa, M. (2017). WGNE intercomparison of tropical cyclone forecasts by operational NWP models: A quarter century and beyond. *Bulletin of the American Meteorological Society*, *98*(11), 2337–2349. doi:10.1175/BAMS-D-16-0133.1

Geophysical Research Letters

Supporting Information for

Large ensemble simulation for investigating predictability of precursor vortex of Typhoon Faxai in 2019 with a 14-km mesh global nonhydrostatic atmospheric model

Y. Yamada[1], T. Miyakawa[2], M. Nakano[1], C. Kodama[1], A. Wada[3], T. Nasuno[1], Y. Chen[2], A. Yamazaki[1], H. Yashiro[4], M. Satoh[2]

[1]Japan Agency for Marine-Earth Science and Technology.

[2]Atmosphere and Ocean Research Institute, the University of Tokyo.

[3]Meteorological Research Institutes, Japan Meteorological Agency.

[4]National Institute for Environmental Studies.

Contents of this file

Introduction

This file includes additional details on vortex tracking (Text S1) and the classification of Faxai-like vortices into type-AB and type-B vortices (Text S2). Figure S1 shows a sample of the classification. Figure S2 shows strike probability densities for type-B vortex. Figure S3 shows the horizontal distribution of 100-member ensemble mean relative vorticity at 850 hPa and the position of Faxai-like vortices 24 h after starting the simulation. Figure S4 shows the ensemble mean central pressures of Faxai-like vortices around the genesis position of Faxai and Tokyo

Bay. Figure S5 shows the ensemble mean time difference between Faxai and Faxai-like vortices around the genesis position of Faxai and Tokyo Bay. Table S1 lists the names of vortices used in this study. Table S2 shows the position information of Pre-Faxai in the EDA.

Text S1. Vortex tracking.

We regarded a local maximum of relative vorticity at an 850-hPa altitude as a candidate for TCs. To find the local maximum, the vorticity field at the 850-hPa altitude was calculated every 6 h using a 1.25° mesh data that was regridded from the original 14-km mesh data for NICAM simulations and the original 25-km mesh data for ERA5. In this study, we ignored the local maxima of which the relative vorticity was less than 1.0×10^{-6} s^{-1}. The local maxima locations were modified using the vorticity field with the 14-km mesh data for NICAM 1600-member ensemble simulation and 25-km mesh data for ERA5. The location of vortex for NICAM climatology ensemble simulation was modified using the sea level pressure field with 14-km mesh data because of a limitation of data storage. We searched for the local minimum sea level pressure in 14-km mesh data around the local maximum relative vorticity in 1.25° mesh data. Next, to create a path, these locations were connected in a time direction by taking a nearest-neighbor approach considering the surrounding flow at 850- and 200-hPa altitudes. We assume the path had to last at least 96 h because the real Faxai took 96 h between genesis and approaching Tokyo Bay. Among the determined paths, those which satisfy the following three conditions for 36 h or longer once or more along the track were defined as the "TC" tracks.

1. The wind speed at 10 m with the original data exceeds 17.5 m s^{-1}.
2. The vorticity at 850 hPa with the 1.25° mesh data exceeds 3.5×10^{-5} s^{-1}.
3. The sum of temperature anomalies at 700, 500, and 300 hPa with the 1.25° mesh data exceeds 2 K.

Those which do not satisfy the above criteria are called "tropical depression" tracks.

Text S2. Faxai-like vortex

We selected Faxai-like vortices from the tracking data described in Text S1. First, we searched for a Faxai-like vortex using a method similar to that of Nakano et al. (2015) applied to the tracking data. The real Faxai was recorded as upgrading to tropical storm intensity at 18 UTC on September 4, 2019, on a location (18.5°N, 156.7°E). We regarded the time as the genesis time of Faxai and the location as the genesis location. Following the method of Nakano et al. (2015), we imposed a criterion for the genesis, which requires passage within a 1000-km radius of the genesis location within 5 days before and after the genesis time, to detect a Faxai-like vortex from the tracking data for each ensemble member. The criterion was called criterion B. We regarded the vortex that satisfied criterion B as a Faxai-like vortex. The minimum distance between the genesis location of the real Faxai and simulated vortex track is defined as DR_B [km], and the time difference at the minimum distance is defined as DT_B [h]. The score for criterion B (S_B) is calculated as follows:

$$S_B = 1 - \frac{DR_B}{1000}\frac{DT_B}{120}. \quad (1)$$

In this study, we discuss not only the genesis but also the subsequent track of Faxai. Because the real Faxai passed over Tokyo Bay (35.3°N, 139.7°E) at 18 UTC on September 8, 2019, we defined the time as the approaching time of Faxai, and the location as the approaching location. For this reason, we also defined criterion A, in which a passage within a 1,000-km radius of the approaching location within 5 days before and after the approaching time is required in addition to criterion B. As with criterion A, a score for criterion A (S_A) was defined as follows:

$$S_A = 1 - \frac{DR_A}{1000}\frac{DT_A}{120}. \quad (2)$$

In the main text, Faxai-like vortices can be classified into two-type vortices: type-AB vortex (satisfying both criteria A and B) and type-B vortex (satisfying only criteria B). We select only one Faxai-like vortex from each ensemble member. When two or more type-AB vortices were detected in an ensemble member, we selected the type-AB vortex with the highest product of the scores for criteria A and B ($S_A \times S_B$). When there is no type-AB vortex in an ensemble member, we selected a type-B vortex as a Faxai-like vortex. When two or more type-B vortices exist, the vortex with the greatest S_B is selected as the Faxai-like vortex. Fig. S1 shows samples of type-AB and type-B vortices.

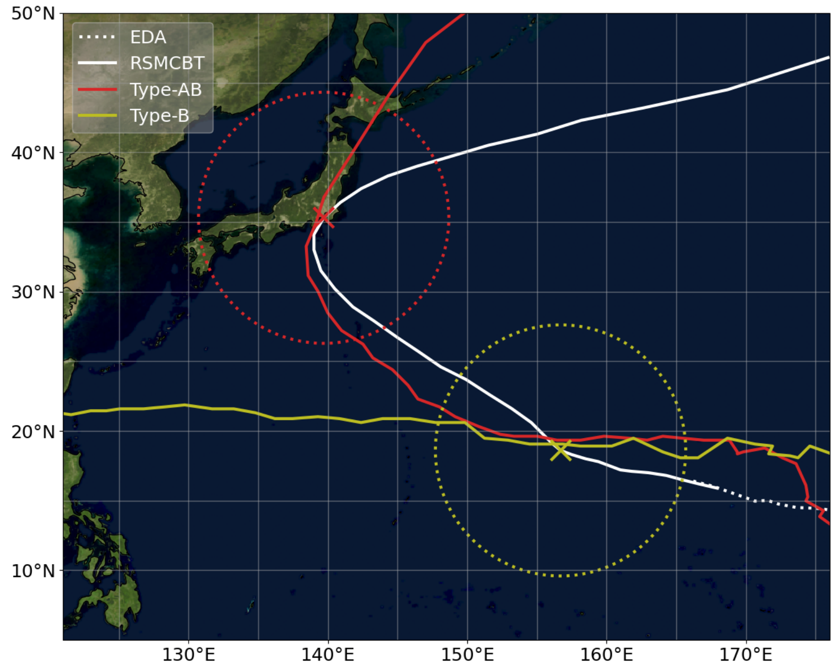

Figure S1. Samples of type-AB and type-B vortex tracks. The red and yellow lines indicate samples of type-AB and type-B vortex tracks respectively. The red and yellow crosses indicate the locations of Faxai genesis (18.5°N, 156.7°E) and Tokyo Bay (35.3°N, 139.7°E), respectively. The red and yellow dotted lines indicate areas within a 1000-km radius of the genesis location and Tokyo Bay, respectively. The white solid and dashed lines represent the RSMCBT and EDA, respectively. Topography and bathymetry are Blue Marble: Next generation (September) which was produced by Reto Stöckli, NASA Earth Observatory.

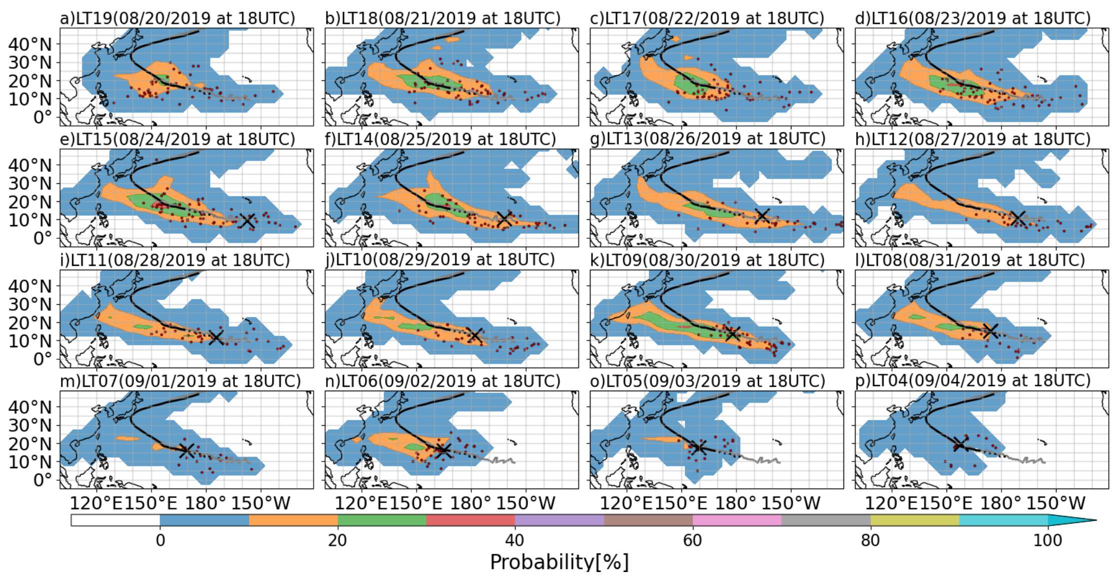

Figure S2. Plan views of strike probability densities for type-B vortex for each 100-member simulation starting from each LT. The density was defined by vortices per 5° cap. The black solid, black dotted, and solid gray lines represent the RSMCBT, the EDA, and ERA5, respectively. The figures in parentheses indicate the start time of each 100-member ensemble simulation. The cross symbol indicates the location of Pre-Faxai (e–o) or Faxai (p) at the start time for each LT. These locations were determined from ERA5. The red circles indicate the starting points of type-AB vortex tracks.

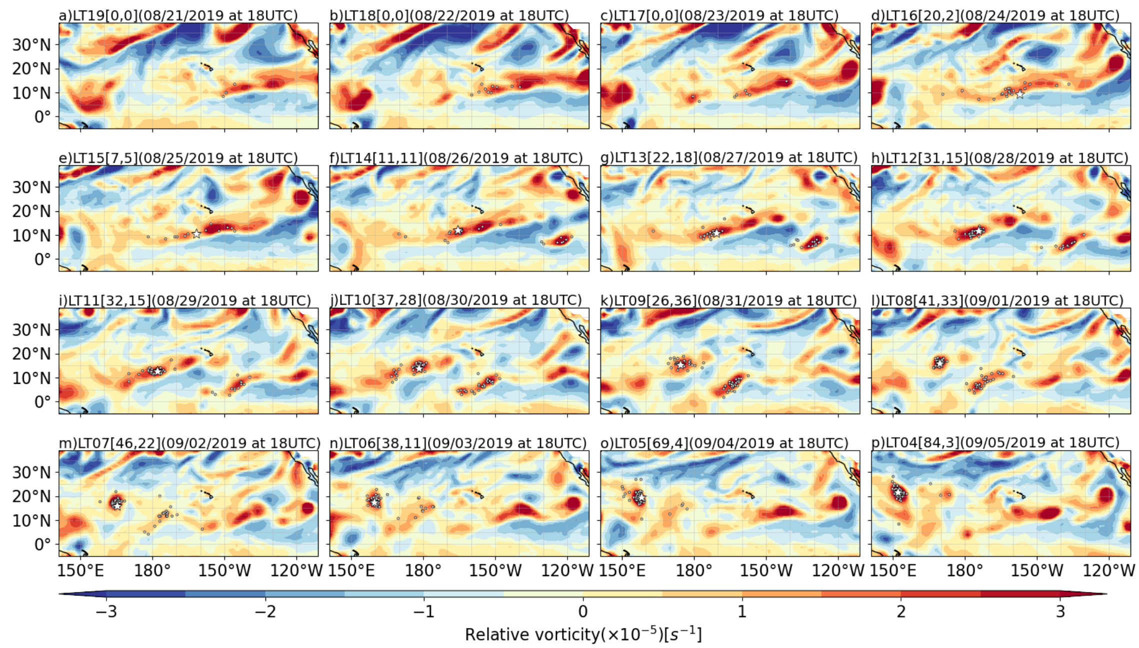

Figure S3. Plan views of the 100-member ensemble mean relative vorticity at 850 hPa at 24 h after the start of simulation for each LT. The figures in parentheses on the panels indicate forecast time. Numerals in square brackets denote the number of vortices originated from the correct vortex at the forecast time, and that originated from the possible vortex. Faxai-like vortices were classified into correct and possible vortices based on the relative position to the real Faxai at the forecast time. A vortex located more than 5° east far from the position of the real Faxai was regarded as a possible vortex. Positions of Faxai-like vortices at the forecast time are embedded on each panel with circles. The star-shaped symbol is the positions of Pre-Faxai (d–n) and Faxai (o and p) analyzed in the ERA5 at the same time as the forecast time.

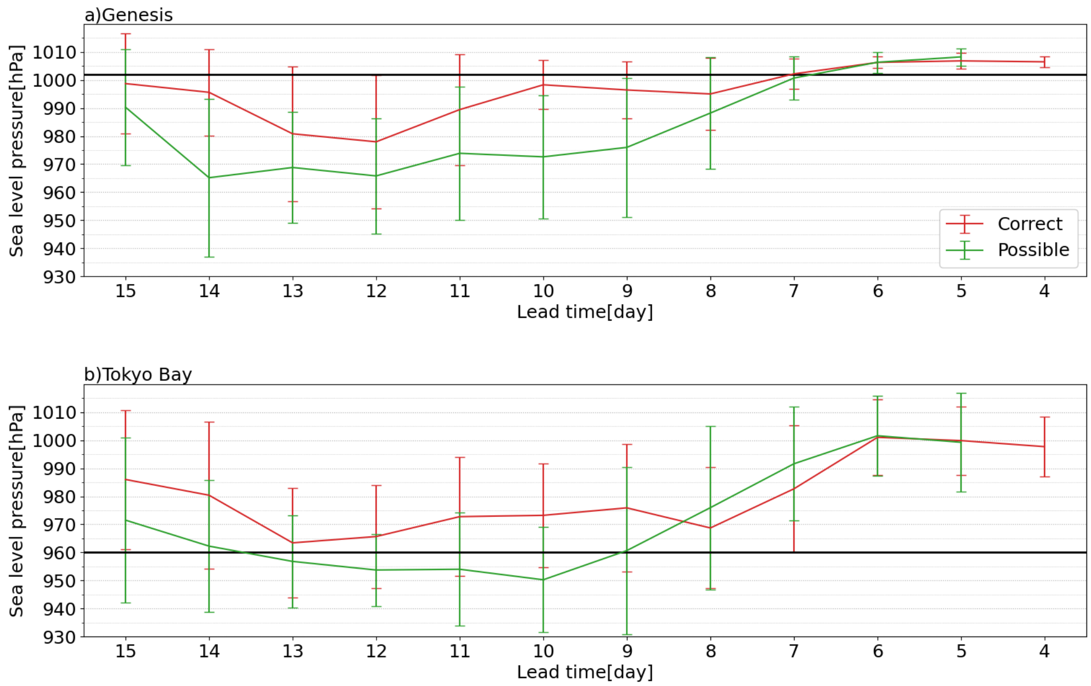

Figure S4. Ensemble mean central pressure of Faxai-like vortices for each LT. The error bars indicate the standard deviation (1− σ). (a) The central pressure of the vortex at the time when the vortex is closest to the genesis location of Faxai (18.5°N, 156.7°E). (b) The central pressure of the vortex at the time when the vortex is closest to the location of Faxai approaching Japan (Tokyo Bay; 35.3°N, 139.7°E). The red and green indicate vortices originated from the correct and possible vortices, respectively. We regarded a vortex whose starting location of the track was more than 5° east far from the location detected in ERA5 at the same time as a correct vortex. The other vortices were regarded as possible vortices.

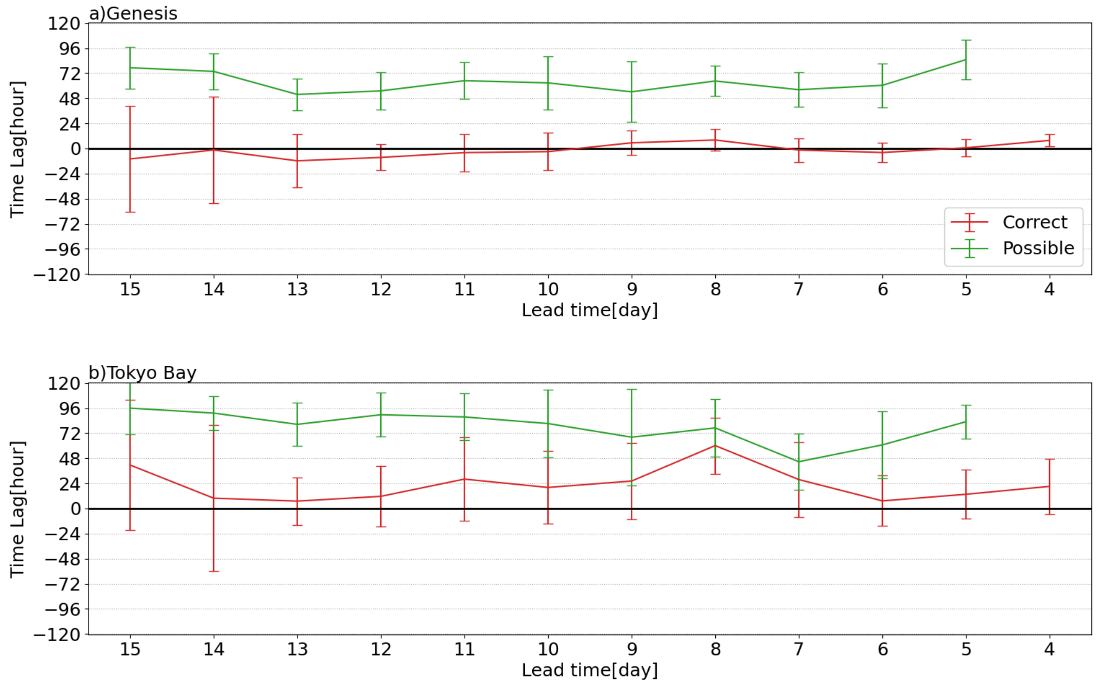

Figure S5. Ensemble mean time difference of Faxai-like vortices for each LT. The error bars indicate the standard deviation. (a) The difference between the genesis time of Faxai (18 UTC on September 4, 2019) and the time when the Faxai-like vortex is closest to the genesis location of Faxai (18.5°N, 156.7°E). (b) The difference between the time of Faxai approaching Tokyo Bay (18 UTC on September 8, 2019) and the time when the Faxai-like vortex is closest to Tokyo Bay (35.3°N, 139.7°E). The red and green indicate vortices originated from the correct and possible vortices, respectively. We regarded a vortex whose starting location of the track was more than 5° east far from the location detected in ERA5 at the same time as a correct vortex. The other vortices were regarded as possible vortices.

Table S1. Names of the vortices used in this study.

Name	Description
Faxai	Typhoon in 2019 caused severe hazards in the Tokyo metropolitan area.
Pre-Faxai	Vortex is the precursor vortex of Faxai, which was recorded in the RSMCBT between 12 UTC on September 4 and 00 UTC on September 2, 2019, the EDA between 6 UTC on September 2 and 12 UTC on August 29, 2019, and detected from ERA5 between 12 UTC on September 4 and 6 UCT on August 24, 2019.
type-AB vortex	Vortex in the ensemble simulation satisfying criteria A and B
type-B vortex	Vortex in the ensemble simulation satisfying only criteria B.
Faxai-like vortices	Vortices in the ensemble simulation, including type-AB and type-B vortices.
correct vortex	Faxai-like vortex originated from a precursor near Pre-Faxai.
Possible vortex	Faxai-like vortex originated from a precursor on the southeast side of Pre-Faxai.

Table S2. Positions of the Pre-Faxai based on the EDA.

Time [UTC]	Latitude [°]	Longitude [°]
2019-08-29T12	12.56	-177.36
2019-08-29T18	12.68	-178.84
2019-08-30T00	12.93	-179.55
2019-08-30T06	12.58	179.76
2019-08-30T12	12.94	179.00
2019-08-30T18	13.22	178.12
2019-08-31T00	13.82	177.52
2019-08-31T06	14.21	176.85
2019-08-31T12	14.44	175.14
2019-08-31T18	14.50	173.64
2019-09-01T00	14.76	172.30
2019-09-01T06	15.01	171.58
2019-09-01T12	14.96	170.64
2019-09-01T18	15.10	170.28
2019-09-02T00	16.03	167.63
2019-09-02T06	16.40	166.20